EEET ECOLOGICAL ENGINEERING & ENVIRONMENTAL TECHNOLOGY

Ecological Engineering & Environmental Technology 2024, 25(9), 54–67
https://doi.org/10.12912/27197050/190108
ISSN 2299–8993, License CC-BY 4.0

Received: 2024.06.14
Accepted: 2024.07.10
Published: 2024.08.01

Monitoring Agricultural Drought in Savanna Ecosystems Using the Vegetation Health Index – Implications of Climate Change

Ketut Dharma Susila[1], Ni Made Trigunasih[1*], Moh Saifulloh[2]

[1] Soil Sciences and Environment Faculty of Agriculture Udayana University, Pb Sudirman Street, Denpasar, Indonesia
[2] Spatial Data Infrastructure Development Center (PPIDS) Udayana University, Pb Sudirman Street, Denpasar, Indonesia
* Corresponding author's e-mail: dharmasusila@unud.ac.id

ABSTRACT

This study aims to monitor the implications of climate change on savanna ecosystem drought using time series data from the Landsat 8 sensor, spanning from 2013 to 2022. We employed a remote sensing computational approach with the semi-automatic classification plugin (SCP) in the open-source QGIS software. Specifically, we utilized channels from the operational land imager (OLI), including Band 4 Red (0.636–0.673 µm) and Band 5 Near-Infrared (0.851–0.879 µm), as well as Thermal Infrared Sensor (TIRS) channels Band 10 TIRS-1 (10.60–11.19 µm) and Band 11 TIRS-2 (11.50–12.51 µm). These channels were used to calculate the vegetation health index (VHI) using the raster calculator, followed by data reclassification with specific thresholds to compare drought-affected areas. Our findings reveal a significant impact of climate change on savanna ecosystem drought over the decade, with the most extreme conditions observed in 2015 and 2019, where drought coverage reached 42.74% and 26.58%, respectively. Other years exhibited relatively low drought dynamics, affecting less than 3% of the area. This period aligns with the el niño-southern oscillation (ENSO) phenomenon, particularly the transition from El Niño to La Niña, known to cause global weather variations, and significantly influenced by the positive phase of the Indian Ocean dipole (IOD). The novelty of this research lies in two main aspects: firstly, the use of Landsat satellite sensors for this specific region has not been extensively studied before; secondly, the discovered impacts of drought in relation to global climate change phenomena are particularly noteworthy. A limitation of this study is the relatively short investigation period of just one decade, which does not fully capture the long-term impacts of climate change. Future research is recommended to utilize imagery with higher temporal resolution over extended periods to better represent extreme climate events and derive drought patterns over durations exceeding one decade.

Keywords: landsat 8 OLI/TIRS, el niño-southern oscillation (ENSO), Indian Ocean dipole (IOD), time series analysis, remote sensing, climate change mitigation.

INTRODUCTION

Global climate change has increasingly exacerbated the frequency and intensity of drought events, profoundly affecting agricultural productivity and ecosystem stability worldwide. These impacts are particularly pronounced in savanna ecosystems, where prolonged periods of water scarcity can lead to significant vegetation stress and soil degradation. Monitoring these drought dynamics is crucial for developing effective mitigation and adaptation strategies. This research focuses on the Bali savanna ecosystems, employing the vegetation health index (VHI) derived from Landsat 8 OLI/TIRS imagery to track and analyze extreme agricultural drought under the influences of climate change from 2013 to 2022.

The environmental issues in the study area are relatively complex, with previous research primarily focusing on agricultural soil science through field observations and laboratory analyses. These studies have covered topics such as soil erosion mapping (Trigunasih and Saifulloh, 2023), landslides (Diara et al., 2022, 2023), soil

fertility levels (Bhayunagiri and Saifulloh 2022; Trigunasih et al., 2023), land degradation (Kartini et al., 2023), flood overflow in the watershed (Suyarto et al., 2023) and the use of remote sensing data to monitor the effects of volcanic eruptions (Trigunasih et al., 2023a), as well as environmental monitoring and their relation to climate variability (Adnyana et al., 2024; Sunarta and Saifulloh, 2022a, 2022b). Previous researchers have noted that the study area is relatively arid and barren, attributed to the annual increase in land surface temperatures. This region even exhibits the highest temperature spots on a regional scale within Bali (Sunarta et al., 2022). This research gap underscores the need to investigate land drought using land surface temperature data and vegetation indices from remote sensing satellites. Addressing this gap will enhance the database and provide new insights into environmental monitoring and disaster mitigation. By leveraging remote sensing technology, this study aims to contribute to a deeper understanding of drought dynamics, which is crucial for developing future mitigation strategies.

The use of remote sensing data is relatively effective, efficient, cost-effective, and requires minimal effort for environmental monitoring and drought disaster monitoring. Remote sensing technology, particularly the operational land imager (OLI) and thermal infrared sensor (TIRS) aboard the Landsat satellite series (Ridwan et al., 2018; Wulder et al., 2019; Xu, 2015), has revolutionized our ability to monitor and analyze environmental phenomena, with a specific focus on vegetation health and drought dynamics (Guha et al., 2018; Sekertekin and Bonafoni, 2020). Numerous studies published in esteemed journals have consistently highlighted the efficacy and utility of Landsat OLI/TIRS data, providing invaluable insights into the nuanced inter-annual variations of drought-affected ecosystems and their dynamics within unique landscapes (Ejaz et al., 2023).

The Landsat program, a collaborative endeavor between NASA and the USGS initiated in the 1970s, has been pivotal in delivering high-fidelity Earth observation data to researchers globally. With the introduction of landsat 8 in 2013, equipped with advanced OLI and TIRS sensors, our capacity for vegetation monitoring and drought assessment has reached unprecedented levels (Hemati et al., 2021; Ridwan et al., 2018). The OLI sensor, renowned for its enhanced spatial resolution, facilitates the capture of multispectral imagery, enabling meticulous analysis of vegetation properties and health indicators (Ke et al., 2015; Masek et al., 2020). Conversely, the TIRS sensor, specializing in thermal infrared radiation measurement, provides vital information on land surface temperatures (Barsi et al., 2014), a critical indicator of vegetation stress and prevailing drought conditions (Nugraha et al., 2019) within complex savanna ecosystems.

The effectiveness of Landsat OLI/TIRS data in vegetation drought mapping has been demonstrated by various researchers, as noted by Ejaz et al. (2023). By integrating spectral indices derived from OLI bands and thermal data from TIRS, researchers have achieved precise assessments of vegetation health and identification of drought-affected regions. This holistic approach to drought monitoring, combining multispectral and thermal data, is particularly significant in regions prone to water stress, such as the savanna areas of Bali. Furthermore, research by Dzakiyah et al. (2022) and Sari et al. (2021) has highlighted the potential of Landsat OLI/TIRS imagery in the early detection of drought-induced vegetation stress. Through detailed time-series analysis, temporal patterns of vegetation response to drought events have been revealed, empowering stakeholders with timely insights for effective mitigation and adaptive management strategies.

Building on these foundational findings, this research aims to harness remote sensing technology, specifically leveraging Landsat 8 imagery, to unravel the complex inter-annual dynamics of drought across the Bali Savanna ecosystem. Employing rigorous quantitative analysis techniques from 2013 to 2022 and guided by established methodologies (Kogan, 2001), the study seeks to map inter-annual drought dynamics using the vegetation health index (VHI). By capitalizing on the high temporal resolution of Landsat 8 imagery, the research aims to detect subtle changes in vegetation health and land surface temperatures, which serve as reliable indicators of drought stress within the diverse savanna ecosystem. Integrating optical and thermal sensor data, the research aspires to provide nuanced insights into the impacts of climate change on drought dynamics. Ultimately, this endeavor aims to inform the development of more effective drought monitoring and adaptation strategies tailored to the unique environmental context of savanna ecosystems, thereby contributing to the preservation and resilience of these ecosystems and their communities.

DATA AND METHODS

Research case study

The Bali Savanna ecosystem encompasses the entirety of the Kubu District, geographically situated between the coordinates 8°10'04.1" – 8°18'12.2" south Latitude and 115°27'11.9" – 115°36'50.5" east Longitude. Within the Kubu District, there are nine villages: Tianyar, Tianyar Barat, Tianyar Tengah, Kubu, Baturinggit, Sukadana, Dukuh, Ban, and Tulamben. This district shares its borders with the Abang District to the east, Mount Agung to the south, Bangli Regency and Buleleng Regency to the west, and the Bali Strait to the north. In total, the research area spans an expansive 23,241.24 hectares, encompassing a diverse range of landscapes and ecosystems within the Kubu District. The precise delineation of the research area is illustrated in Figure 1, providing a visual representation of the geographical extent under investigation.

Image acquisition

The materials for this study were obtained from the USGS Earth Explorer website (https://earthexplorer.usgs.gov/). The dataset utilized consisted of Landsat 8 imagery spanning from 2013 to 2022, capturing images during one day of the dry season each year. Data processing and analysis were conducted as part of the study, with accuracy testing carried out using correlation analysis between soil moisture, rainfall data, and the extent of drought from 2013 to 2022.

Landsat 8's primary mission is surface monitoring, aimed at understanding the management of resources crucial for sustaining humanity, such as food, water, and forests. This involves monitoring environmental impacts and changes among other objectives. Landsat 8 imagery comprises 11 bands, including visible, near infrared (NIR), short wave infrared (SWIR), panchromatic, and thermal bands. Bands 1 through 7 and 9 have a spatial resolution of 30 meters, while band 8 has a spatial resolution of 15 meters. Bands 10 and 11 have a coarser spatial resolution of 100 meters (Roy et al., 2014). Each band serves a specific purpose in analyzing Landsat imagery, and combinations of bands are necessary to obtain imagery suitable for the desired analysis theme or purpose. Details of the operational land imager (OLI) and thermal infrared sensor (TIRS) onboard Landsat 8 are provided in Table 1.

Satellite image processing

Image processing involves the utilization of the QGIS 3.34.5 LTR application (https://qgis.org/en/site/), specifically version 3.28 Long Term Release, equipped with the Semi-Automatic Classification Plugin (SCP) (https://

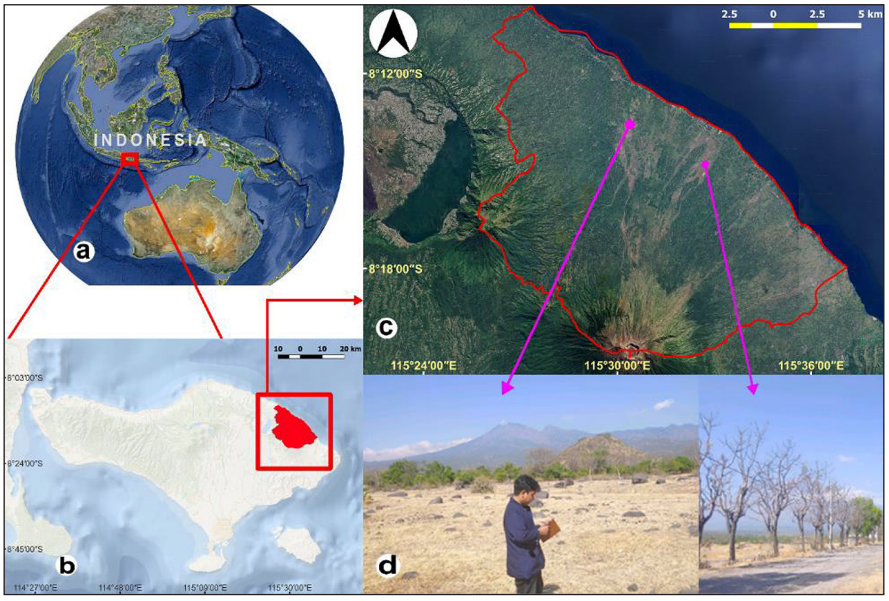

Figure 1. Depicts the research location viewed from different scales: the research site falls within Indonesia (a), it is situated in the province or island of Bali, with the research area delineated in the red zone located in the northeast of the island (b), the research utilizes the 2020 Google Earth base map to visualize the Bali Savanna Ecosystem features (c), additionally, field conditions were investigated by researchers in 2019 (d)

Table 1 Landsat 8 OLI/TIRS image specifications

Sensors	Bands	Wavelength (μm)	Resolution (m)
Operational land imager (OLI)	Band 1 – coastal aerosol	0.43 – 0.45	30
	Band 2 – blue	0.45 – 0.51	30
	Band 3 – green	0.53 – 0.59	30
	Band 4 – red	0.64 – 0.67	30
	Band 5 – near infrared (NIR)	0.85 – 0.88	30
	Band 6 – shortwave infrared (SWIR) 1	1.57 – 1.65	30
	Band 7 – shortwave infrared (SWIR) 2	2.11 – 2.29	30
	Band 8 – panchromatic	0.50 – 0.68	15
	Band 9 - cirrus	1.36 – 1.38	30
Thermal infrared sensor (TIRS)	Band 10 – thermal infrared (TIRS) 1	10.60 – 11.19	100
	Band 11 – (TIRS) 2	11.50 – 12.51	100

plugins.qgis.org/plugins/SemiAutomaticClassificationPlugin/) for comprehensive pre-processing, processing, and post-processing of satellite images. At the pre-processing stage, dark object subtraction image correction, available within SCP, is employed to enhance the quality of the imagery data. Prior to further processing or performing raster calculations on spectral bands, all data undergoes projection into the WGS 84/UTM zone 50s coordinate system, or with authority ID EPSG 32750, ensuring spatial consistency and accuracy.

Subsequently, the imagery data is meticulously interpreted to identify various vegetation and temperature-related indices, crucial for assessing environmental conditions and vegetation health. Notably, normalized difference vegetation index (NDVI) and vegetation condition index (VCI) are computed from Landsat 8 imagery data, capturing the conditions during each dry season. Additionally, land surface temperature (LST) and temperature condition index (TCI) are derived from Landsat 8 imagery data spanning the years 2013–2022 on an annual basis. These datasets are then processed by summation to obtain the annual LST values, providing insights into temperature variations over time.

Moreover, the vegetation healthy index (VHI) is computed through the combination of TCI with VCI utilizing the raster calculator feature within QGIS. This index offers a comprehensive assessment of vegetation health by integrating temperature conditions with vegetation conditions. The computation of each parameter is guided by specific equations tailored to capture the nuances of environmental dynamics and vegetation responses over the study period. These meticulous processes ensure accurate and reliable data analysis, enabling robust insights into the dynamics of vegetation health and environmental conditions across the study area.

The vegetation index can be calculated using the Equation 1, proposed by (Rouse et al., 1973; Tucker, 1979), which is as follows Eq. 1:

$$\mathrm{NDVI} = \frac{(NIR - red)}{(NIR + red)} \tag{1}$$

where: NIR is near-infrared radiation from the pixex, red is red light radiation from the pixel

The VCI index is related to the long-term minimum and maximum values of NDVI, whereas the TCI index is associated with the long-term minimum and maximum values of LST. VCI is calculated using the following Eq. 2:

$$VCI = \frac{NDVI - NDVImin}{NDVImax + NDVI} \times 100\% \tag{2}$$

where: NDVI is the NDVI value in a particular year, NDVImin is the long-term minimum NDVI value and NDVImax is the long-term maximum NDVI value

To calculate TCI, the following Eq. 3, is used: LST data is utilized to depict the thermal influence/surface temperature on plant health because high temperatures lead to low humidity, causing plants to undergo stress. LST employs the average of Bands 10 and 11 from Landsat 8 and calculated using the following Eq. 3.

$$LST = \frac{BT}{1 + \frac{(BT \times \lambda)}{c} \times ln\,\varepsilon} \tag{3}$$

where: LST is Land surface temperature (°C), BT is the top of atmosphere brightness temperature, λ is the wavelength of emitted radiance, c is the speed of light, and ε is the land surface emissivity. Next, the calculated LST results are utilized to compute the TCI as outlined in formula 4.

$$TCI = \frac{LSTmax - LST}{LSTmax + LSTmin} \times 100\% \quad (4)$$

where: TCI is the TCI value in a specific year, LSTmin is the long-term minimum LST value and LSTmax is the long-term maximum LST value

The VHI value is obtained from the combination of VCI and TCI indices. The calculation of the VHI index can be done with the Formula 5:

$$VHI = (0.5 \times VCI) + (0.5 \times TCI) \quad (5)$$

According to (Kogan, 2001), due to the unclear contribution of humidity and temperature in the vegetation cycle, it is assumed that the weights of VCI and TCI are equal or balanced, i.e., 0.5 each.

Classification of drought levels

This process is conducted after image processing and the calculation of the VHI index. Subsequently, the method adopted from (Kogan, 2001) involves grouping the VHI index into five drought classes. The results of this grouping are utilized in the data classification stage. The criteria for VHI index values for each drought class are presented in Table 2.

RESULT AND DISCUSSIONS

Inter-annual NDVI and LST

The normalized difference vegetation index (NDVI) represents vegetation density, health, and the level of greenness of plants. NDVI values range from -1 to 1, with values closer to 1 indicating high levels of greenness and vegetation density, while values closer to -1 indicate non-vegetated areas such as water bodies, bare land, and built-up areas (Huang et al., 2021; Pettorelli et al., 2005, 2011). As shown in Figure 2, the lowest average NDVI occurred in 2020, while the highest average was observed in 2016. This suggests that, overall, the average vegetation in the Bali Savanna is relatively healthy and not excessively poor.

The land surface temperature (LST) represents the temperature level on the surface, where higher values indicate hotter surface temperatures and lower values indicate cooler surface temperatures (Hijmans et al., 2005; Li et al., 2013; Rayner et al., 2003). Figure 2 illustrates that the highest temperatures occurred in 2015, whereas the lowest temperatures were recorded in 2020. This trend is also evident in the heat levels displayed in Figure 2, indicating significant heat exposure in the years 2015 and 2019. When comparing the average NDVI and LST in Figure 3, differences in the increase of LST and the decrease of NDVI can be observed. For example, in 2015 and 2019, there was a decrease in NDVI accompanied by an increase in LST. This comparison highlights a reduction in vegetation density, as indicated by the decrease in NDVI, coupled with a significant increase in LST, leading to drought conditions. Such data comparisons can effectively indicate the occurrence of drought disasters in specific years.

The relationship between near-infrared (NIR), red, and thermal infrared sensor (TIRS) bands, as well as the derived NDVI and LST, holds significant implications for understanding drought dynamics in savanna ecosystems. In savanna regions, vegetation plays a critical role in regulating water availability and maintaining ecosystem balance. During periods of drought, vegetation undergoes stress due to limited water availability, leading to changes in its physiological and spectral properties. The NIR and Red bands, captured

Table 2 Classification of drought levels

No	VHI value	Description
1	< 10	Severe drought
2	10 < 20	Moderate drought
3	20 < 30	Mild drought
4	30 < 40	Slight drought
5	> 40	No drought occurrence

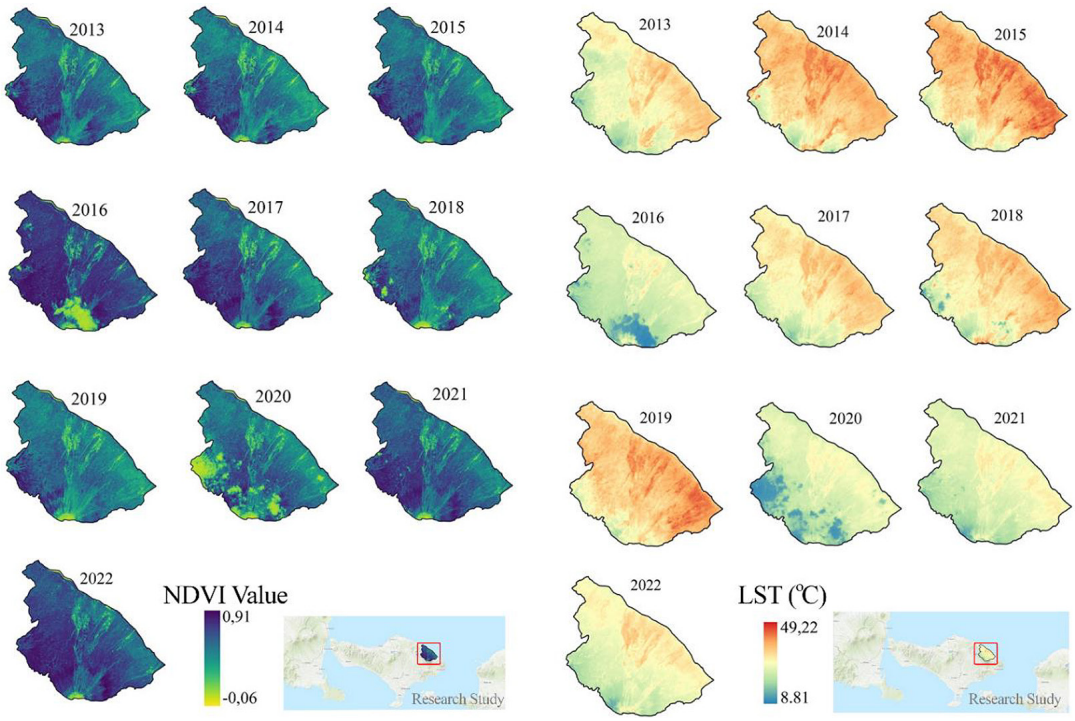

Figure 2. Inter-annual spatial distribution of NDVI and LST

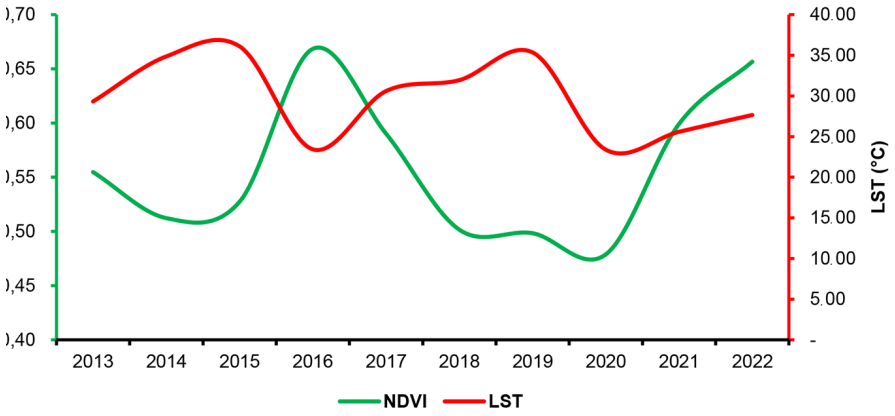

Figure 3. Graph of the relationship between the mean NDVI value and LST

by sensors like Landsat 8 OLI/TIRS, are sensitive to these changes, reflecting alterations in vegetation density and health.

The NDVI, calculated from NIR and Red bands (Huang et al., 2021), serves as a robust indicator of vegetation condition and drought stress in savannas. Decreases in NDVI values often correspond to reductions in vegetation greenness and density, signalling drought-induced vegetation stress (Dzakiyah et al., 2022; Pettorelli et al., 2005). In savanna ecosystems, prolonged drought can result in widespread vegetation decline, impacting ecosystem services such as carbon sequestration, soil stabilization, and biodiversity conservation (Morales-Rincon et al., 2021; Sankaran, 2019; Staver et al., 2019; Zhang and Yuan, 2020).

Simultaneously, LST, derived from TIRS data, provides insights into land surface temperature variations associated with drought conditions. During drought events, land surface temperatures tend to rise due to reduced evaporative cooling from vegetation transpiration (Hazaymeh and Hassan, 2017; Wolteji et al., 2022). Consequently, areas experiencing drought stress exhibit elevated LST values, indicating thermal anomalies and heightened surface heating. The relationship between NDVI and LST during drought periods in savannas is intricate

and dynamic. As vegetation experiences water stress and declines in density, NDVI values decrease, while LST values tend to increase due to decreased evaporative cooling and increased absorption of solar radiation by the bare ground. This inverse relationship between NDVI and LST serves as a valuable tool for monitoring drought impacts on savanna ecosystems.

Inter-annual VCI and TCI

The vegetation condition index (VCI) serves as a method for extracting and discerning weather-related components within NDVI values, thereby acting as a seasonal risk assessment tool. VCI offers diverse spatial and temporal vegetation insights closely linked to local weather patterns, making it a pivotal vegetation index and drought indicator. Utilizing the interpretation of vegetation health index (VHI), wherein values below certain thresholds signify varying degrees of drought severity, VCI enables the assessment of drought conditions. For instance, an indicator of < 10 suggests severe drought, < 20 indicates moderate drought, < 30 reflects mild drought, and values > 40 indicate no drought. Analysis presented in Table 4 across the years 2013–2022 reveals that no area exceeding 23,000 hectares experienced drought, hence indicating that VCI alone may not suffice as a primary indicator. Nonetheless, as illustrated in Figure 4, some regions did encounter mild drought in 2015, despite the absence of concurrent temperature indicators. Therefore, to enhance accuracy, VCI calculations should incorporate temperature indicators.

The temperature condition index (TCI) serves as an indicator derived from LST, offering insights into the temperature conditions over vegetation cover. TCI plays a crucial role in conjunction with the VCI to identify drought occurrences in savanna area. TCI's connection with VCI enables the indication of drought occurrence, aligning with interpretations from the VHI indicator, as illustrated in Table 2. However, it's noteworthy that drought occurrences depicted in TCI surpass those in VCI, highlighting that TCI solely reflects surface temperature and has yet to be integrated with the VCI indicator. Consequently, TCI does not currently serve as a primary indicator in this research

The utilization of the TCI alongside the VCI provides a comprehensive approach to assessing drought occurrences in the savanna area. While VCI primarily reflects vegetation health and stress, TCI offers valuable insights into surface temperature dynamics, which are critical factors influencing vegetation response to drought. Integrating these indices allows for a more nuanced understanding of drought dynamics, considering both vegetation conditions and temperature variations.

The vegetation health index

The vegetation health index (VHI) serves as the primary indicator utilized for classifying land drought through remote sensing methodologies. This parameter, drawn from Kogan (2001), assumes a central role in this research for assessing drought occurrences. The outcomes of drought classification are presented in Table 5, elucidating that drought manifested most prominently in 2015 and 2019. Specifically, in 2015, mild drought affected 30.66% (7,126.02 ha) of the Savanna Bali area, moderate drought impacted 10.83% (2,517.66 ha), and severe drought was observed in 1.24% (288.99 ha) of the region (Table 4). Research by Lorenzo and Mantua (2016), Jiménez-Muñoz et al. (2016), and Oliveira de Morais et al. (2021) states that these occurrences align with the El Niño climate phenomenon, characterized by reduced rainfall and desiccated soil conditions.

Similarly, in 2019, mild drought affected 25.72% (5,977.98 ha) of the Savanna ecosystem, with moderate drought impacting 0.8% (199.44 ha). This condition is caused by the impact of the positive Indian Ocean dipole (IOD+)

Table 3. Statistical data on areas experiencing drought based on the vegetation condition index (VCI)

Drought categories	VCI 2013	VCI 2014	VCI 2015	VCI 2016	VCI 2017	VCI 2018	VCI 2019	VCI 2020	VCI 2021	VCI 2022
Severe	0.09	0.18	7.2	0.09	0.27	0.45	0.09	0.18	0.27	0.09
Moderate	0	1.53	73.44	0.09	1.17	3.06	0.09	0.54	0.72	0
Mild	0.18	9.63	331.38	0	7.2	20.43	0.09	2.43	5.58	0
Slight	0	72.9	686.07	0.09	23.67	75.69	1.44	43.29	20.61	0.09
No drought	23,240.97	23.157	22.143.15	23,240.97	23,209.38	23,141.61	23,239.53	23,194.8	23,214.06	23,241.06

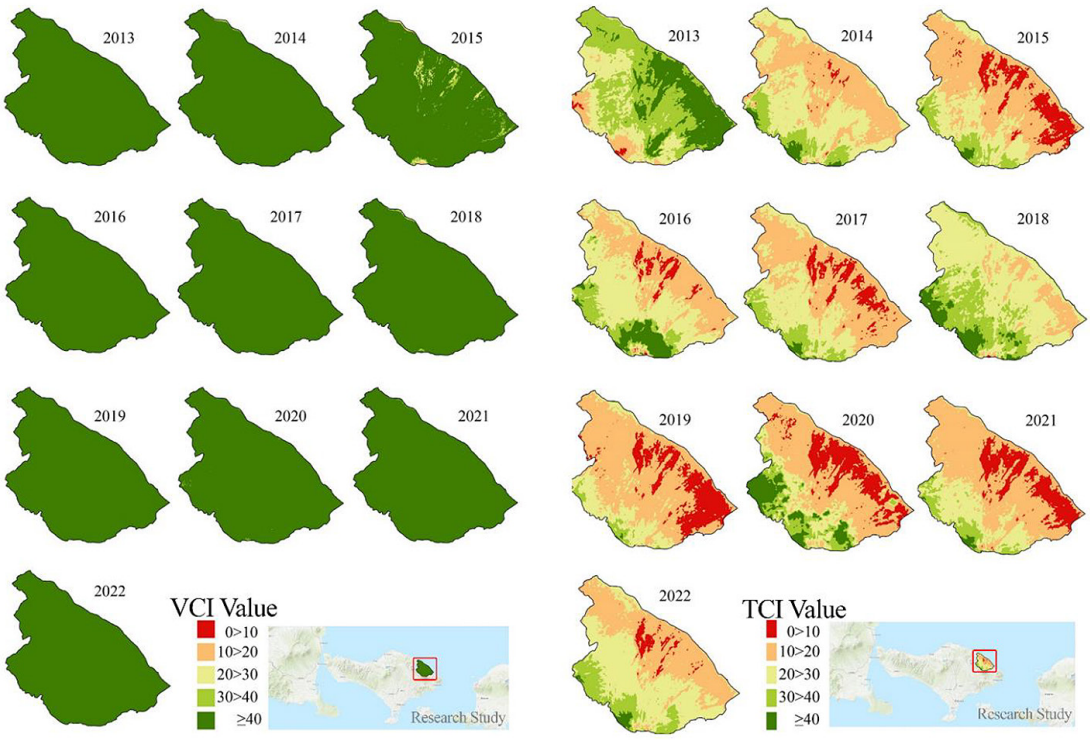

Figure 4. Inter-annual spatial distribution of drought based on VCI and TCI

Table 4 Statistical data on areas experiencing drought based on the temperature condition index (TCI)

Drought categories	TCI 2013	TCI 2014	TCI 2015	TCI 2016	TCI 2017	TCI 2018	TCI 2019	TCI 2020	TCI 2021	TCI 2022
Severe	176.58	229.41	3,451.68	1,036.8	2,094.75	13.32	4,497.66	4,212.45	3,842.73	840.24
Moderate	1,433.07	9,962.1	12,029.22	8,136.72	11,300.04	2,609.37	13,868.64	10,722.78	12,761.46	9,199.62
Mild	5,567.22	10,033.83	5,616.81	9,836.28	7,501.23	13,166.64	4,173.93	3,410.46	4,875.39	10,014.39
Slight	10,002.24	2,439	1,925.91	2,407.59	2,102.22	5,569.02	6,69.06	2,516.04	1,554.66	2,842.83
No drought	6,062.13	585	217.62	1,823.85	243	1,891.89	31.95	2,379.51	207	344.16

phenomenon during this period (Arfaansyah et al., 2021; Irfan and Iskandar, 2022), although its intensity was notably lower compared to 2015. Table 4 also highlights sporadic instances of severe drought, albeit at relatively lower levels. Additionally, Figure 4.5 illustrates widespread drought occurrences across Savanna Bali in 2015 and 2019, with several points experiencing severe drought conditions in 2015. Conversely, in 2014, 2018, and 2020, mild drought was observed, albeit confined to a few zones on the map (Figure 5).

Effect of climate change on agricultural drought

The implications of climate change are starkly evident in savanna ecosystem, as demonstrated by the dynamics of changes in the area experiencing drought over the past decade (Figure 6). One of the most significant impacts was observed during the transition from 2015 to 2016, where 42.74% of the area experienced drought. This severe drought was followed by a notable recovery in vegetation, reducing the drought-affected area to less than 1%. This period coincided with the el niño-southern oscillation (ENSO) phenomenon, specifically the transition from El Niño to La Niña, which is known to cause extreme weather variations globally.

Moreover, the effects of climate change were also apparent in the drought dynamics around 2019. Prior to and following this year, the drought-affected area was less than 3%. However, in 2019, the area experiencing drought surged to 26.58%. This dramatic increase was not only influenced by the ENSO event but was also significantly impacted by the positive phase of the Indian Ocean dipole (IOD). The positive IOD, characterized by

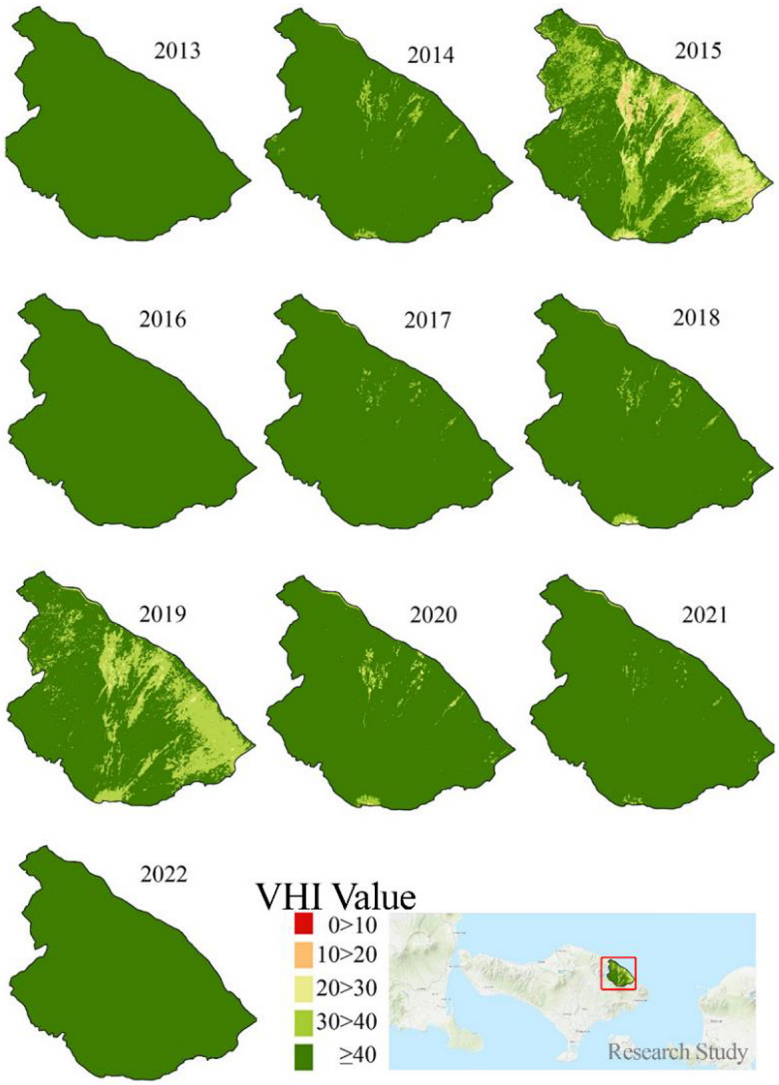

Figure 5. Inter-annual drought dynamics map based VHI

warmer sea surface temperatures in the western Indian Ocean relative to the eastern part, typically exacerbates drought conditions in surrounding regions, including the savannas of Bali.

These observations underscore the compounded effects of climate change and interannual climate variability, such as ENSO and IOD, on drought dynamics. The interplay between these phenomena leads to more frequent and severe drought events, highlighting the urgent need for comprehensive monitoring and adaptive management strategies. Understanding these climate drivers and their impacts on savanna ecosystems is crucial for developing effective mitigation and adaptation strategies to enhance the resilience of these ecosystems in the face of ongoing climate change. Such insights are vital for policymakers and conservationists working towards sustainable management and conservation of vulnerable ecosystems affected by climate variability and long-term climate trends.

The savanna biome, characterized by its blend of grasses and scattered trees, is highly susceptible to shifts in precipitation patterns and temperature regimes, particularly under the influence of climate change (Jobbágy and Jackson, 2000; Räsänen et al., 2017). This susceptibility exacerbates the frequency and severity of drought events, placing added stress on savanna ecosystems and prompting significant alterations in vegetation structure, composition, and distribution (Gang et al., 2016; Nippert and Holdo, 2015; Wilcox et al., 2020).

Recent studies have emphasized the intricate relationship between climate variability, drought occurrence, and changes in savanna vegetation (Bergstrom et al., 2023; Irob et al., 2023). For instance, the extreme El Niño event of 2015 resulted

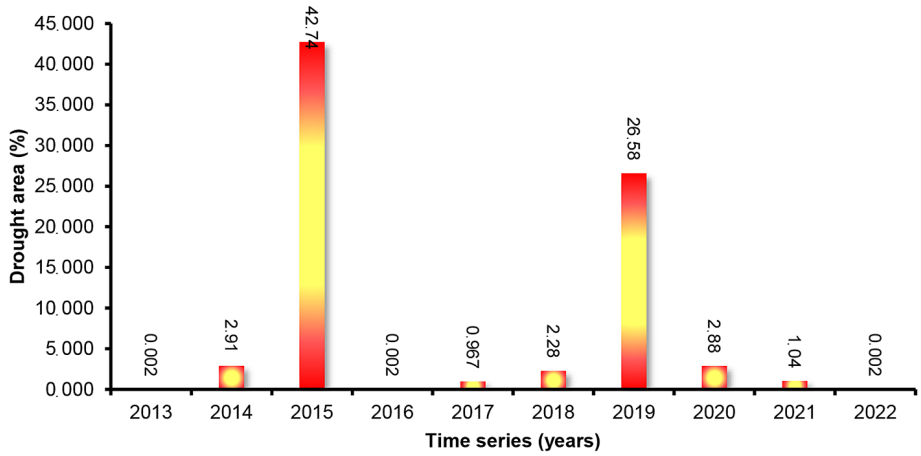

Figure 6. Graph of the percentage of area experiencing drought due to climate change in Savanna ecosystems. Note: The percentage of drought areas is derived from the total of four drought categories: slight, mild, moderate, and severe

Table 5 Statistical data on areas experiencing drought based on the vegetation health index (VHI)

Drought categories	VHI 2013	VHI 2014	VHI 2015	VHI 2016	VHI 2017	VHI 2018	VHI 2019	VHI 2020	VHI 2021	VHI 2022
Severe	0	0	0	0	0.09	0	0.09	0.09	0.09	0
Moderate	0.09	0.18	288.99	0.18	0.45	0.27	0.18	0.45	0.72	0.09
Mild	0	18.9	2,517.66	0.09	12.15	40.05	199.44	76.41	21.51	0.09
Slight	0.36	656.28	7,126.02	0.09	211.95	489.33	5,977.98	593.55	219.42	0.18
No drought	23,240.79	22,565.88	14,118.57	23,240.88	22,986	22,711.59	17,063.55	22,570.74	22,999.5	23,240.88

in widespread water scarcity and extended dry spells across the savanna landscape, significantly impacting vegetation health (Mbatha and Xulu, 2018). This period saw reduced foliage density, increased leaf senescence, and heightened susceptibility to wildfires. Similarly, the IOD+ event in 2019 exacerbated drought conditions, further testing the resilience of savanna vegetation.

Remote sensing technologies, such as Landsat 8 OLI/TIRS imagery, play a pivotal role in monitoring and assessing the impacts of drought on savanna ecosystems. By capturing high-resolution data on vegetation indices and land surface temperatures, these satellite-based observations offer valuable insights into the spatial and temporal dynamics of drought-induced vegetation stress. Integrating such data derived from OLI and TIRS sensors allows researchers to quantify the extent of drought impacts, identify vulnerable areas, and prioritize conservation efforts effectively.

Based on high-resolution Google Earth imagery, the year 2019, characterized by the positive phase of the Indian Ocean Dipole (IOD+), exhibited significant vegetation stress, indicative of severe drought conditions. However, contrasting this, the La Niña event in 2022 facilitated a recovery in vegetation, demonstrating improved vegetation health and reduced drought stress. This stark contrast between years of extreme drought and subsequent recovery underscores the profound impact of extreme climate variability on the savanna ecosystem (Figure 7).

Climate change has increasingly exacerbated the frequency and intensity of drought events, profoundly affecting agricultural productivity and ecosystem stability worldwide. These impacts are particularly pronounced in savanna ecosystems, where prolonged periods of water scarcity can lead to significant vegetation stress and soil degradation. Monitoring these drought dynamics is crucial for developing effective mitigation and adaptation strategies.

Apart from direct ecological consequences, drought-induced changes in savanna vegetation can have profound socio-economic implications for local communities reliant on these ecosystems for livelihoods and ecosystem services. Reduced pasture productivity, for example, can undermine livestock grazing activities, leading to economic losses and food insecurity. Additionally, alterations in vegetation cover and structure can affect water availability, soil fertility, and carbon

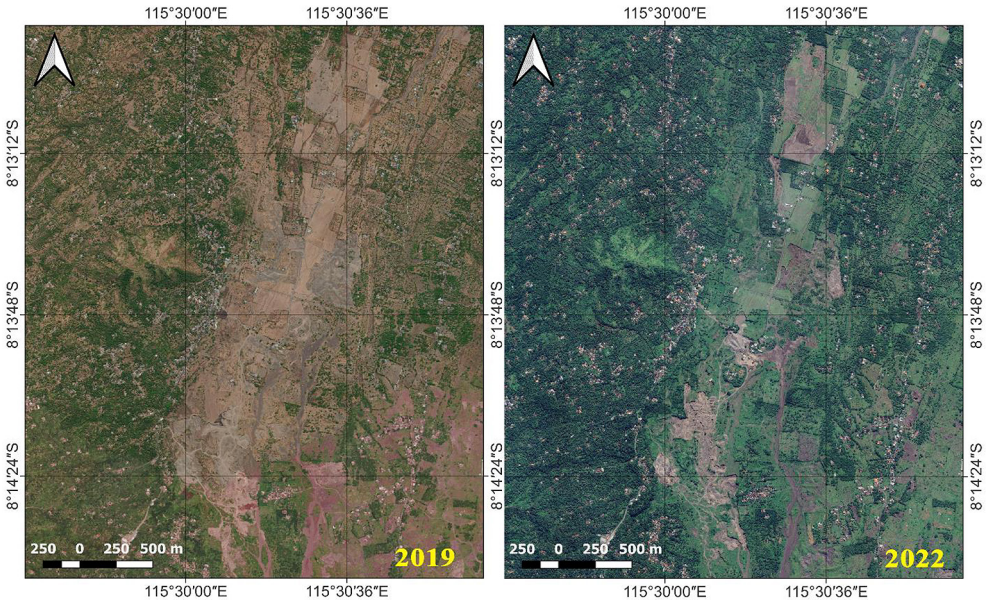

Figure 7. Implications of climate change for drought in savanna ecosystems as shown in Google Earth Imagery for 2019 and 2022

sequestration capacities, exacerbating vulnerabilities in the face of climate change.

Integrating remote sensing data with predictive modelling techniques also enables the development of early warning systems for drought detection and monitoring. By leveraging the predictive power of remote sensing technologies, stakeholders can anticipate and respond to emerging drought risks promptly, minimizing the socio-economic impacts on local communities and ecosystems. Collaborative efforts among researchers, policymakers, and local communities are essential to co-design and implement context-specific mitigation strategies addressing the unique challenges posed by inter-annual drought dynamics in the savanna landscape of Bali.

CONCLUSIONS

The monitoring of extreme agricultural drought in the savanna ecosystem, utilizing the vegetation health index under the effects of climate change, revealed significant insights through the analysis of Landsat 8 OLI/TIRS time series imagery. Our study underscores the profound impact of climate variability on vegetation health, particularly during the extreme dryness induced by the el niño and positive Indian Ocean dipole events in 2015 and 2019. These climate phenomena resulted in significant drought conditions, which were subsequently alleviated during the La Niña periods, demonstrating a clear link between climate change and vegetation stress. Through the application of remote sensing technology, our study provided valuable insights into the drought dynamics of the savanna, contributing to informed decision-making for conservation and management efforts in the face of climate change.

Acknowledgements

This research did not receive funding from any institution, including governmental, for-profit, or non-profit organizations. We extend our sincere gratitude to NASA for providing free access to time-series remote sensing data, which greatly facilitated our analysis of the effects of climate change on extreme drought. We also wish to thank the anonymous reviewers for their valuable suggestions and feedback on this manuscript.

REFERENCES

1. Adnyana, I.W.S., As-syakur, A.R., Suyarto, R., Sunarta, I.N., Nuarsa, I.W., Diara, I.W., Saifulloh, M., Wiyanti. 2024. Geospatial Technology for Climate Change: Influence of ENSO and IOD on Soil Erosion. In Technological Approaches for Climate Smart Agriculture, p. 249–275 Springer.
2. Arfaansyah, T., Putut, I., Dimyati, M. 2021. Agricultural drought identification based on Soil Moisture Index (SMI) during 2019 Indian Ocean dipole (IOD) in Bekasi Regency. https://doi.

org/10.1117/12.2623397

3. Barsi, J.A., Schott, J.R., Hook, S.J., Raqueno, N.G., Markham, B.L., Radocinski, R.G. 2014. Landsat-8 thermal infrared sensor (TIRS) vicarious radiometric calibration. Remote Sensing, 6(11). https://doi.org/10.3390/rs61111607
4. Bergstrom, B.J., Scruggs, S.B., Vieira, E.M. 2023. Tropical savanna small mammals respond to loss of cover following disturbance: A global review of field studies. In Frontiers in Ecology and Evolution (Vol. 11). https://doi.org/10.3389/fevo.2023.1017361
5. Bhayunagiri, I.B.P., Saifulloh, M. 2022. Mapping of Subak Area Boundaries and Soil Fertility for Agricultural Land Conservation. Geographia Technica, 17(2). https://doi.org/10.21163/GT_2022.172.17
6. Diara, I.W., Suyarto, R., Saifulloh, M. 2022. Spatial distribution of landslide susceptibility in new road construction Mengwitani-Singaraja, Bali-Indonesia: based on geospatial data. International Journal of GEOMATE, 23(96). https://doi.org/10.21660/2022.96.3320
7. Diara, I.W., Wahyu Wiradharma, I.K.A., Suyarto, R., Wiyanti, W., Saifulloh, M. 2023. Spatio-temporal of landslide potential in upstream areas, Bali tourism destinations: remote sensing and geographic information approach. Journal of Degraded and Mining Lands Management, 10(4). https://doi.org/10.15243/jdmlm.2023.104.4769
8. Dzakiyah, I.F., Saraswati, R., Pamungkas, F.D. 2022. The Potential of Agricultural Land Drought Using Normalized Difference Drought Index in Ciampel Subdistrict Karawang Regency. International Journal on Advanced Science, Engineering and Information Technology, 12(3). https://doi.org/10.18517/ijaseit.12.3.13261
9. Ejaz, N., Bahrawi, J., Alghamdi, K.M., Rahman, K.U., Shang, S. 2023. Drought Monitoring Using Landsat Derived Indices and Google Earth Engine Platform: A Case Study from Al-Lith Watershed, Kingdom of Saudi Arabia. Remote Sensing, 15(4). https://doi.org/10.3390/rs15040984
10. Gang, C., Wang, Z., Chen, Y., Yang, Y., Li, J., Cheng, J., Qi, J., Odeh, I. 2016. Drought-induced dynamics of carbon and water use efficiency of global grasslands from 2000 to 2011. Ecological Indicators, 67. https://doi.org/10.1016/j.ecolind.2016.03.049
11. Guha, S., Govil, H., Dey, A., Gill, N. 2018. Analytical study of land surface temperature with NDVI and NDBI using Landsat 8 OLI and TIRS data in Florence and Naples city, Italy. European Journal of Remote Sensing, 51(1). https://doi.org/10.1080/22797254.2018.1474494
12. Hazaymeh, K., Hassan, Q.K. 2017. A remote sensing-based agricultural drought indicator and its implementation over a semi-arid region, Jordan. Journal of Arid Land, 9(3). https://doi.org/10.1007/s40333-017-0014-6
13. Hemati, M., Hasanlou, M., Mahdianpari, M., Mohammadimanesh, F. 2021. A systematic review of landsat data for change detection applications: 50 years of monitoring the earth. In Remote Sensing 13(15). https://doi.org/10.3390/rs13152869
14. Hijmans, R.J., Cameron, S.E., Parra, J.L., Jones, P. G., Jarvis, A. 2005. Very high resolution interpolated climate surfaces for global land areas. International Journal of Climatology, 25(15). https://doi.org/10.1002/joc.1276
15. Huang, S., Tang, L., Hupy, J.P., Wang, Y., Shao, G. 2021. A commentary review on the use of normalized difference vegetation index (NDVI) in the era of popular remote sensing. In Journal of Forestry Research 32(1). https://doi.org/10.1007/s11676-020-01155-1
16. Irfan, M., Iskandar, I. 2022. The impact of positive iod and la niña on the dynamics of hydroclimatological parameters on peatland. International Journal of Geomate, 23(97). https://doi.org/10.21660/2022.97.3307
17. Irob, K., Blaum, N., Weiss-Aparicio, A., Hauptfleisch, M., Hering, R., Uiseb, K., Tietjen, B. 2023. Savanna resilience to droughts increases with the proportion of browsing wild herbivores and plant functional diversity. Journal of Applied Ecology, 60(2). https://doi.org/10.1111/1365-2664.14351
18. Jiménez-Muñoz, J.C., Mattar, C., Barichivich, J., Santamaría-Artigas, A., Takahashi, K., Malhi, Y., Sobrino, J.A., Schrier, G. Van Der. 2016. Record-breaking warming and extreme drought in the Amazon rainforest during the course of El Niño 2015-2016. Scientific Reports 6. https://doi.org/10.1038/srep33130
19. Jobbágy, E.G., Jackson, R.B. 2000. The vertical distribution of soil organic carbon and its relation to climate and vegetation. Ecological Applications, 10(2). https://doi.org/10.1890/1051-0761(2000)010[0423:TVDOSO]2.0.CO;2
20. Kartini, N.L., Saifulloh, M., Trigunasih, N.M., Narka, I.W. 2023. Assessment of soil degradation based on soil properties and spatial analysis in dryland farming. Journal of Ecological Engineering, 24(4). https://doi.org/10.12911/22998993/161080
21. Ke, Y., Im, J., Lee, J., Gong, H., Ryu, Y. 2015. Characteristics of Landsat 8 OLI-derived NDVI by comparison with multiple satellite sensors and in-situ observations. Remote Sensing of Environment, 164. https://doi.org/10.1016/j.rse.2015.04.004
22. Kogan, F.N. 2001. Operational space technology for global vegetation assessment. Bulletin of the American Meteorological Society, 82(9). https://doi.org/10.1175/1520-0477(2001)082<1949:OSTFGV>2.3.CO;2
23. Li, Z.L., Tang, B.H., Wu, H., Ren, H., Yan, G., Wan, Z., Trigo, I.F., Sobrino, J.A. 2013. Satellite-derived

land surface temperature: Current status and perspectives. Remote Sensing of Environment, 131. https://doi.org/10.1016/j.rse.2012.12.008

24. Lorenzo, E., Mantua, N. 2016. Multi-year persistence of the 2014/15 North Pacific marine heatwave. Nature Climate Change, 6(11). https://doi.org/10.1038/nclimate3082
25. Masek, J.G., Wulder, M.A., Markham, B., McCorkel, J., Crawford, C.J., Storey, J., Jenstrom, D.T. 2020. Landsat 9: Empowering open science and applications through continuity. Remote Sensing of Environment, 248. https://doi.org/10.1016/j.rse.2020.111968
26. Mbatha, N., Xulu, S. 2018. Time series analysis of MODIS-Derived NDVI for the Hluhluwe-Imfolozi Park, South Africa: Impact of recent intense drought. Climate, 6(4). https://doi.org/10.3390/cli6040095
27. Morales-Rincon, L.A., Hernandez, A.J., Rodriguez-Hernandez, N.S., Jimenez, R. 2021. Carbon Exchange and Accumulation in an Orinoco High Plains Native Savanna Ecosystem as Measured by Eddy Covariance. Frontiers in Environmental Science, 9. https://doi.org/10.3389/fenvs.2021.673932
28. Nippert, J.B., and Holdo, R.M. 2015. Challenging the maximum rooting depth paradigm in grasslands and savannas. Functional Ecology, 29(6). https://doi.org/10.1111/1365-2435.12390
29. Nugraha, A.S.A., Gunawan, T., Kamal, M. 2019. Comparison of Land Surface Temperature Derived from Landsat 7 ETM+ and Landsat 8 OLI/TIRS for Drought Monitoring. IOP Conference Series: Earth and Environmental Science, 313(1). https://doi.org/10.1088/1755-1315/313/1/012041
30. Oliveira de Morais, T.M., Berenguer, E., Barlow, J., França, F., Lennox, G.D., Malhi, Y., Chesini Rossi, L., Maria Moraes de Seixas, M., Ferreira, J. 2021. Leaf-litter production in human-modified Amazonian forests following the El Niño-mediated drought and fires of 2015–2016. Forest Ecology and Management, 496. https://doi.org/10.1016/j.foreco.2021.119441
31. Pettorelli, N., Ryan, S., Mueller, T., Bunnefeld, N., Jedrzejewska, B., Lima, M., Kausrud, K. 2011. The normalized difference vegetation index (NDVI): Unforeseen successes in animal ecology. In Climate Research, 46(1). https://doi.org/10.3354/cr00936
32. Pettorelli, N., Vik, J.O., Mysterud, A., Gaillard, J.M., Tucker, C.J., Stenseth, N.C. 2005. Using the satellite-derived NDVI to assess ecological responses to environmental change. In Trends in Ecology and Evolution, 20(9). https://doi.org/10.1016/j.tree.2005.05.011
33. Räsänen, M., Aurela, M., Vakkari, V., Beukes, J.P., Tuovinen, J.P., Van Zyl, P.G., Josipovic, M., Venter, A.D., Jaars, K., Siebert, S.J., Laurila, T., Rinne, J., Laakso, L. 2017. Carbon balance of a grazed savanna grassland ecosystem in South Africa. Biogeosciences, 14(5). https://doi.org/10.5194/bg-14-1039-2017
34. Rayner, N.A., Parker, D.E., Horton, E.B., Folland, C.K., Alexander, L.V., Rowell, D.P., Kent, E.C., Kaplan, A. 2003. Global analyses of sea surface temperature, sea ice, and night marine air temperature since the late nineteenth century. Journal of Geophysical Research: Atmospheres, 108(14). https://doi.org/10.1029/2002jd002670
35. Ridwan, M.A., Radzi, N.A.M., Ahmad, W.S.H.M.W., Mustafa, I.S., Din, N.M., Jalil, Y.E., Isa, A.M., Othman, N.S., Zaki, W.M.D.W. 2018. Applications of landsat-8 data: A Survey. International Journal of Engineering and Technology(UAE), 7(4). https://doi.org/10.14419/ijet.v7i4.35.22858
36. Rouse, J.W., Hass, R.H., Schell, J.A., Deering, D.W. 1973. Monitoring vegetation systems in the great plains with ERTS. Third Earth Resources Technology Satellite (ERTS) Symposium, 1.
37. Roy, D.P., Wulder, M.A., Loveland, T.R.C.E.W., Allen, R.G., Anderson, M.C., Helder, D., Irons, J.R., Johnson, D.M., Kennedy, R., Scambos, T.A., Schaaf, C.B., Schott, J.R., Sheng, Y., Vermote, E.F., Belward, A.S., Bindschadler, R., Cohen, W.B., Gao, F., Zhu, Z. 2014. Landsat-8: Science and product vision for terrestrial global change research. Remote Sensing of Environment, 145. https://doi.org/10.1016/j.rse.2014.02.001
38. Sankaran, M. 2019. Droughts and the ecological future of tropical savanna vegetation. In Journal of Ecology, 107(4). https://doi.org/10.1111/1365-2745.13195
39. Sari, Y.A., Sriartha, I.P., Adi Nugraha, A.S. 2021. Mapping The drought area through Landsat 8 OLI/TIRS With LST Model SWA-S Method in Banyuwangi Regency. https://doi.org/10.4108/eai.9-9-2021.2314836
40. Sekertekin, A., Bonafoni, S. 2020. Land surface temperature retrieval from Landsat 5, 7, and 8 over rural areas: Assessment of different retrieval algorithms and emissivity models and toolbox implementation. Remote Sensing, 12(2). https://doi.org/10.3390/rs12020294
41. Staver, A.C., Wigley-Coetsee, C., Botha, J. 2019. Grazer movements exacerbate grass declines during drought in an African savanna. Journal of Ecology, 107(3). https://doi.org/10.1111/1365-2745.13106
42. Sunarta, I.N., Saifulloh, M. 2022a. Coastal Tourism: Impact for Built-Up Area Growth and Correlation to Vegetation and Water Indices Derived From Sentinel-2 Remote Sensing Imagery. Geojournal of Tourism and Geosites, 41(2). https://doi.org/10.30892/gtg.41223-857
43. Sunarta, I.N., Saifulloh, M. 2022b. Spatial variation of NO_2 levels during the covid-19 pandemic in

the Bali Tourism Area. Geographia Technica, 17(1). https://doi.org/10.21163/GT_2022.171.11

44. Sunarta, I.N., Suyarto, R., Saifulloh, M., Wiyanti, W., Susila, K.D., Kusumadewi, L.G.L. 2022. Surface urban heat island (SUHI) phenomenon in Bali and Lombok tourism areas based on remote sensing. Journal of Southwest Jiaotong University, 57(4). https://doi.org/10.35741/issn.0258-2724.57.4.44
45. Suyarto, R., Wiyanti, Saifulloh, M., Fatahillah, A.W., Diara, I.W., Susila, K.D., Kusmiyarti, T. B. 2023. Hydrological approach for flood overflow estimation in Buleleng Watershed, Bali. International Journal of Safety and Security Engineering, 13(5). https://doi.org/10.18280/ijsse.130512
46. Trigunasih, N.M., Narka, I.W., Saifulloh, M. 2023a. Mapping eruption affected area using Sentinel-2A imagery and machine learning techniques. Journal of Degraded and Mining Lands Management, 11(1). https://doi.org/10.15243/jdmlm.2023.111.5073
47. Trigunasih, N.M., Narka, I.W., Saifulloh, M. 2023b. Measurement of soil chemical properties for mapping soil fertility status. International Journal of Design and Nature and Ecodynamics, 18(6). https://doi.org/10.18280/ijdne.180611
48. Trigunasih, N.M., Saifulloh, M. 2023. Investigation of Soil Erosion in Agro-Tourism Area: Guideline for Environmental Conservation Planning. Geographia Technica, 18(1). https://doi.org/10.21163/GT_2023.181.02
49. Tucker, C.J. 1979. Red and photographic infrared linear combinations for monitoring vegetation. Remote Sensing of Environment, 8(2). https://doi.org/10.1016/0034-4257(79)90013-0
50. Wilcox, K.R., Koerner, S.E., Hoover, D.L., Borkenhagen, A.K., Burkepile, D.E., Collins, S.L., Hoffman, A.M., Kirkman, K.P., Knapp, A.K., Strydom, T., Thompson, D.I., Smith, M.D. 2020. Rapid recovery of ecosystem function following extreme drought in a south African savanna grassland. Ecology, 101(4). https://doi.org/10.1002/ecy.2983
51. Wolteji, B.N., Bedhadha, S.T., Gebre, S.L., Alemayehu, E., Gemeda, D.O. 2022. Multiple Indices Based Agricultural Drought Assessment in the Rift Valley Region of Ethiopia. Environmental Challenges, 7. https://doi.org/10.1016/j.envc.2022.100488
52. Wulder, M.A., Loveland, T.R., Roy, D.P., Crawford, C.J., Masek, J.G., Woodcock, C.E., Allen, R.G., Anderson, M.C., Belward, A.S., Cohen, W.B., Dwyer, J., Erb, A., Gao, F., Griffiths, P., Helder, D., Hermosilla, T., Hipple, J.D., Hostert, P., Hughes, M.J., Zhu, Z. 2019. Current status of Landsat program, science, and applications. Remote Sensing of Environment, 225. https://doi.org/10.1016/j.rse.2019.02.015
53. Xu, H.Q. 2015. Retrieval of the reflectance and land surface temperature of the newly-launched Landsat 8 satellite. Acta Geophysica Sinica, 58(3). https://doi.org/10.6038/cjg20150304
54. Zhang, M., Yuan, X. 2020. Rapid reduction in ecosystem productivity caused by flash droughts based on decade-long FLUXNET observations. Hydrology and Earth System Sciences, 24(11). https://doi.org/10.5194/hess-24-5579-2020